Multireference Calculations on Bond Dissociation and Biradical Polycyclic Aromatic Hydrocarbons as Guidance for Fractional Occupation Number Weighted Density Analysis in DFT Calculations

Jhonatas R. Carvalho,¹ Reed Nieman,¹ Miklos Kertesz,² Adelia J. A. Aquino,³ Andreas Hansen,⁴* Hans Lischka¹*

¹Department of Chemistry and Biochemistry, Texas Tech University, Lubbock, TX 79409-1061, USA

- ² Chemistry Department and Institute of Soft Matter, Georgetown University, Washington, District of Columbia 20057-1227, USA
- ³ Department of Mechanical Engineering, Texas Tech University, Lubbock, TX 79409-1061, USA
- ⁴ Mulliken Center for Theoretical Chemistry, University of Bonn, Beringstr. 4, 53115 Bonn, Germany

^{*} Email: <u>Hans.Lischka@ttu.edu</u>, <u>hansen@thch.uni-bonn.de</u>

Abstract

This study explores open shell biradical and polyradical molecular compounds based on extended multireference (MR) methods (MR-configuration interaction with singles and doubles (CISD) and MR-averaged quadratic coupled cluster (AQCC) approach) using the numbers of unpaired densities N_U . These results were used to guide the analysis of the fractional occupation number weighted density (FOD) calculated within the finite temperature (FT) density functional theory (DFT) approach. As critical test examples, the dissociation of carbon-carbon (CC) single, double and triple bonds, and a benchmark set of polycyclic aromatic hydrocarbons (PAHs) has been chosen. By examining single, double, and triple bond dissociations, we demonstrate the utility and accuracy but also limitations of the FOD analysis for describing these dissociation processes. In significant extension of previous work (Phys Chem Chem Phys 25: 27380-27393) the assessment of FOD applications for different classes of DFT functionals was performed examining the range-separated functionals ωB97XD, ωB97M-V, CAM-B3LYP, LC-ωPBE, and MN12-SX, the hybrid (M06-2X) functional and the double hybrid (B2P-LYP) functional. In all cases, strong correlations between N_{FOD} and N_{U} values are found. The major task was to develop a new linear regression formula for range-separated functionals allowing a convenient determination of the optimal electronic temperature $T_{\rm el}$ for the FT-DFT calculation. We also established an optimal temperature for the semi-empirical extended tight-binding GFN2-xTB method. These findings significantly broaden the applicability of FOD analysis across various DFT functionals and semi-empirical methods.

1 INTRODUCTION

The aim of this study is to provide guidance for DFT calculations in difficult situations arising from multireference conditions, i.e. in cases where several configurations become quasidegenerate in a wavefunction-based calculation. As important examples, the properties of long CC bonds [1-8], bond dissociation and biradical character of molecules raise interesting questions concerning the use of appropriate methodology and analysis. Because of the open shell structures encountered in such cases, usage of multireference (MR) approaches is considered as most appropriate [9]. However, respective methods are computationally demanding, and finite temperature density functional theory approaches have been proven to be useful to efficiently address even such difficult situations [10-16]. Thereby, the occupation of low-lying virtual orbitals opens a way to address the afore mentioned biradical character of a molecule. Several descriptors are being used for the characterization of open shell character based on natural orbital occupations like unpaired electron densities [17-19], indices separating dynamic and nondynamic electron correlation [20, 21] or other indices to define external electron numbers [22]. Another interesting approach is based on the fractional occupation number weighted density (FOD) analysis [23], which offers a useful chemical approach to provide concrete insight into the biradical properties based on DFT calculations. This method can be considered as simplified adoption of Chai's thermally-assisted-occupation density functional theory (TAO-DFT) [14-16]. In TAO-DFT, a fictitious temperature of the reference system generates fractional orbital occupations via the Fermi-Dirac distribution. Furthermore, it was shown that the static correlation is closely related to the entropy contribution. Neglecting the fictitious-temperaturedependent energy functionals leads to the finite-temperature DFT method (FT-DFT in the following) in the context of the FOD. In FOD calculations the electronic temperature $T_{\rm el}$ enters as a parameter. Originally, a pragmatic empirical formula based on a linear relationship with the amount of exact Fock exchange had been suggested [23]. Recently, this formula for the Tel values has been revised by comparison with the effective numbers of unpaired electrons (N_U) based on MR averaged quadratic coupled cluster (MR-AQCC) [9, 24] calculations, which resulted in excellent agreement between N_U and the fractional occupation numbers, N_{FOD} [10]. In this work the optimized regression formula for T_{el} (cf. Eq. (5)(5) below) was applied to a few selected hybrid functionals, namely TPSS [25], B3LYP [26, 27], and M05-2X [28]. However, its applicability to other classes of density functional approximations such as to range-separated and double-hybrid functionals has not yet been shown. Another important question is the applicability of the FOD analysis to semiempirical methodologies that do not incorporate exact Fock exchange, such as the extended tight-binding (xTB) method [29]. E.g. GFN2-xTB [30] has become quite popular due to its balance of computational efficiency, robustness and reasonable accuracy thus making it suitable for large systems including extended organic molecules, smaller proteins, and cluster structures. Although it is possible to perform the FOD analysis with GFN2-xTB, there is currently no recommendation available for determining $T_{\rm el}$ for this method.

In this work, we aim to address two questions in relation to the use of the FOD approach. One refers to the robustness of the DFT/FT-DFT/FOD approach under severe bi- and polyradical conditions. The other one is the extension of the $T_{\rm el}$ optimization to the above-mentioned additional classes of DFT functionals. The first question will be addressed by studying carbon-carbon (CC) bond dissociation of single, double and triple bonds (see Figure 1 for structures of all compounds investigated in this work). To study single CC bond dissociation, we selected ethane (1) and 9,9'-(ethene-1,1-diyl)bis(9H-fluorene) (2) as a recent interesting example [31] investigated in the challenging quest for long CC single bonds. For double and triple CC bond dissociation, we chose ethylene (3) and acetylene (4), respectively. MR-AQCC reference potential energy curves (PECs) and the evolution of $N_{\rm U}$ values along these curves will be determined to be used for the evaluation of FOD calculations based on restricted (R)DFT and unrestricted (U)DFT approaches. This experience will then be applied to the discussion of the chemically interesting structure 2.

The diversification of functionals for determining optimized $T_{\rm el}$ values for FOD calculations beyond the scope of previous work [10] is the second goal. For this, the range-separated class of DFT functionals such as the popular ω B97XD [32, 33], ω B97M-V [34], CAM-B3LYP [35], LC- ω PBE [36], and MN12-SX [37] approaches will be considered. Additionally, the double hybrid functional B2P-LYP [38] and the popular hybrid functional M06-2X [39] complete this list. As test compounds the following 22 polycyclic aromatic hydrocarbons (PAHs) with singlet ground states from that work, shown in Figure 1, will be used to correlate the $N_{\rm U}$ values calculated previously with MR-AQCC [10] and the number of "hot" electrons ($N_{\rm FOD}$ values) calculate for the above list of DFT functionals. The singlet ground state PAHs from our previous work include the acenes 5 to 8, trans-diindenoacenes (9-13), cisdiindenoacenes (14-18), zethrenes (19-21), fluoroanthene (22), acenaphthylene (23), CH₂-

terminated Chichibabin's hydrocarbon (24), 2,6-anthraquinodimethane (25), and bis-periazulene (26). The results to be presented below will show not only an excellent correlation between N_{FOD} and N_{U} values but, after the rescaling of T_{el} also a very good agreement in actual numbers.

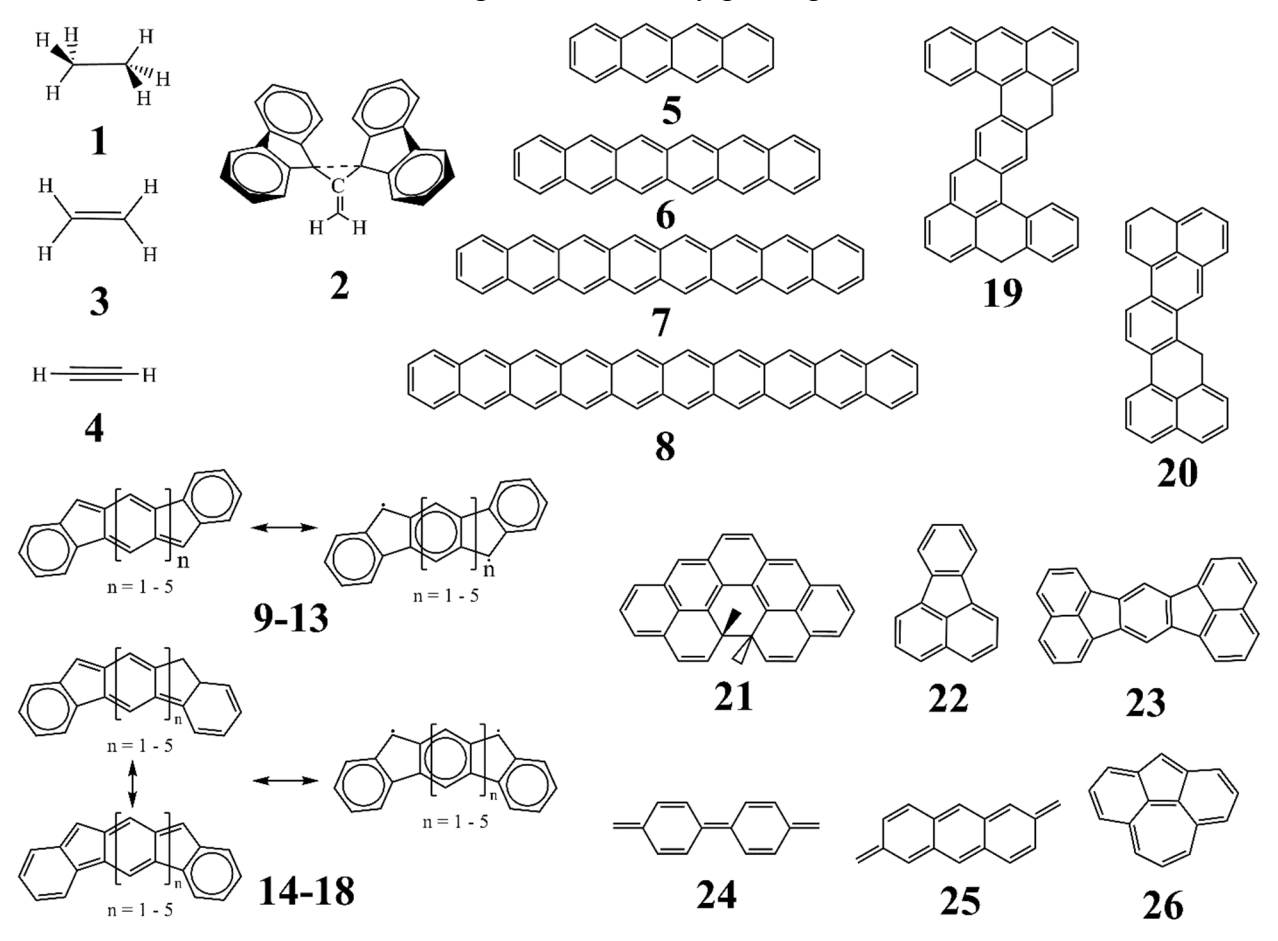


Figure 1. Benchmark structures for the study of the density of unpaired electrons at MR-QCC level in comparison with the FOD analysis using a set of different DFT functionals.

2 COMPUTATIONAL DETAILS

The PECs for relaxed displacement along the CC bonds for the molecules ethane, ethylene, and acetylene as well as their polyradical character were computed at different computational levels. As reference, the MR-AQCC method was used with the following construction of the reference space. The orbitals for these three molecules were computed by a multiconfiguration self-consistent field (MCSCF) calculation using different selections of wavefunctions. The simplest one is based on the perfect-pairing multiconfigurational (PPMC) expansion. This approach is a multiconfiguration self-consistent field method, where the many-electron wavefunction is constructed in the framework of the family of generalized valence bond

- restricted configuration interaction (GVB-RCI) methods [40-43]. PPMC is a direct product wavefunction, in which each pair of electrons is occupying a bonding/antibonding orbital pair allowing only double excitations within each pair. In the case of ethane, the wavefunction is constructed from each bonding and antibonding pair of the CC bond and six C-H bonds. The two 1s core orbitals are restricted to double occupation. This method allows for a smooth dissociation of ethane into the two CH₃ radical fragments. To allow for correct bond dissociation for the PEC of ethylene, the GVB-RCI wavefunction was employed, as it is a generalization of the PPMC wavefunction allowing for all possible open-shell configurations with all possible spin couplings [40-43]. Acetylene is an even more complicated case as it requires also electron redistribution as will be shown in the Results section. In this case, a full valence complete active space using ten electrons and ten orbitals (CAS(10,10)) was used. This calculation was performed in D_{2h} symmetry, where acetylene was oriented along the z axis, with five electronic states in the singlet Ag averaged to investigate avoided crossings within the ground state symmetry. Dynamic electronic correlation was included using the MR-AQCC method [24] for ethane and ethylene. MR-AOCC is a variational approach based on single- and double excitations containing additionally size-consistency contributions. In the case of acetylene, five electronic states were included at the MR-CISD level. As reference wavefunctions the just-mentioned respective PPMC, GVB-RCI and CAS(10,10) wavefunctions were used derived from the respective multiconfiguration self-consistent field (MCSCF) calculations. In the acetylene case, stateaveraging over five states (SA5) was performed.

The polyradical nature was assessed using the MR-AQCC reference approach by means of N_U values and the corresponding unpaired electron density [17, 18] using the nonlinear formula developed by Head-Gordon [19]:

$$N_U = \sum_{i=1}^{N} n_i^2 (2 - n_i)^2 \tag{1}$$

Here, N is the number of natural orbitals (NOs), and n_i is the occupation of the ith NO. This approach emphasizes the orbitals with occupations close to one, while suppressing contributions near 0 and 2. All N_U values for PAHs 5 to 26 used in the correlation analysis were obtained from the previous publication [10]. In that study, the singlet ground states of PAHs were calculated using the MR-AQCC method and the 6-311G(d) [44, 45] basis set. The orbitals for those MR-

AQCC calculations were computed at the CASSCF level, averaging over two states (SA2), the lowest singlet and triplet, utilizing a CAS(8,8) reference space.

The DFT calculations of the relaxed dissociation curves and the zero-point energy (ZPE) correction were performed with the functional B3LYP for structures 1 to 4, since this functional has been found reliable for predicting the structures of Kubo et al [1]. For structures 5-26, geometries have been computed with TPSS and the def2-TZVP [46, 47] basis set. They are available in the SI of Ref. [10]. For the calculation of FOD values at the TPSS geometry the hybrid M06-2X, the double hybrid functional B2P-LYP and the range separated functionals CAM-B3LYP, ω B97XD, LC- ω PBE, MN12-SX, and ω B97M-V were used. A triplet instability [48, 49] analysis was performed for all structures. In case of an instability found, unrestricted (U)DFT calculations were performed as well. In the DFT context, the polyradical character is assessed using the FOD analysis [23] (FOD, ρ FOD) which is performed by means of the FT-DFT approach [14-16] and controls the occupation of the virtual orbitals by adjusting the electronic temperature (T_{el}). In this method, the fractional orbital density is defined as

$$\rho^{\text{FOD}}(r) = \sum_{i}^{N} (\delta_{1} - \delta_{2} f_{i}) |\phi_{i}(r)|^{2}$$
(2)

where δ_1 and δ_2 are constants chosen to be unity if the level is lower than the Fermi energy, E_F , or 0 and -1, respectively, when the level is higher than E_F . The ϕ_i 's are molecular spin orbitals, the sum is taken over all orbitals N. The f_i values are obtained from the Fermi-Dirac distribution with fractional orbital occupation numbers as

$$f_i = \frac{1}{e^{(\varepsilon_i - E_F)/kT_{el}} + 1} \tag{3}$$

with ε_i representing the orbital energy. For GGA, meta-GGA and hybrid DFT functionals, the electronic temperature T_{el} , is taken as a parameter with its value based on the percentage of non-local Fock exchange admixture a_x in the functional. According to the equation suggested in Ref. [23], T_{el} is given as $T_{el} = 20\,000\,\mathrm{K} \cdot a_x + 5\,000\,\mathrm{K}$, or in an improved equation as $T_{el} = 10762\,\mathrm{K} \cdot a_x + 6140\,\mathrm{K}$ [10]. In the present work, a new electronic temperature is proposed for range separated functionals, increasing the temperature in steps of 1000 K and refining in steps of 200 K. The N_{FOD} value is calculated as

$$N_{FOD} = \sum_{i=1}^{N} (\delta_1 - \delta_2 f_i) \tag{4}$$

The N_{FOD} values were also evaluated using the semiempirical Extended Tight-Binding (xTB) methodology [29]. In this work, the N_{FOD} values for structures **5-26** were evaluated using GFN2-xTB [30] parametrization. The correlation between these GNF2-xTB N_{FOD} values and MR-AQCC N_{U} values was used to determine the optimal electronic temperature for this method as well, increasing the temperature in steps of 1000 K and refining in steps of 200 K.

Geometry optimizations, stability analysis and FT-DFT calculations were performed with the TURBOMOLE 7.5 program [50, 51]. FOD analysis for FT-DFT calculation was performed using the foden/Turbomole program [23]. FOD calculations are available also via the ORCA program package [52, 53]. All PPMC, GVB-RCI, and MR-AQCC calculations were performed using the COLUMBUS [54-56] program suite. Extended tight-binding calculations including FOD analysis were performed through the *xtb* software (version 6.3.3).

3 RESULTS AND DISCUSSIONS

3.1. Single CC bond dissociation

The analysis of the evolution of diradical character of CC bond dissociation in ethane sheds light on compounds like tris(9-fluorenylidene)methane introduced by Kubo et al [1], which have been synthesized in the quest for long CC bonds. This section explores FOD calculations for bond dissociation in ethane and a model structure, 9,9'-(ethene-1,1-diyl)bis(9H-fluorene) for Kubo's structures [31].

The evolution of N_U values and the PEC for relaxed displacement of the CC bond in ethane is shown in Figure 2 for the MR-AQCC(PPMC) reference approach. In the dissociation limit, N_U assumes the value 2.0 e, indicating that the CC bond is completely broken and the combination of the two CH₃ radical fragments constitutes a diradical system. Near the equilibrium geometry, the N_U value is practically zero. In this geometry, the calculated carbon-carbon distance, $d_{C-C,eq.}$, is 1.532 Å, while the experimental value is 1.531±0.002 Å [57]. Figure 2Figure 2 shows that the diradical character for the dissociation of the CC bond starts to increase rapidly beyond a CC distance of about 2 Å. At around 4 Å, the CC bond is almost completely dissociated, with the number of unpaired electrons converging to 2 e. The dissociation energy without ZPE correction (D_e) is 93.9 kcal/mol. The calculated dissociation energy D_θ (including ZPE correction) is 84.4 kcal/mol, which agrees quite well with the experimental value of 88.1±2.1 kcal/mol (via heats of formation) [58]. For comparison, from the GVB calculations by

Dunning et al. [59] a D_e value of 80.9 kcal/mol is reported using an aug-cc-pVQZ basis set. This value is significantly smaller than our D_e result using the MR-AQCC(PPMC) showing the importance of including dynamic electron correlation.

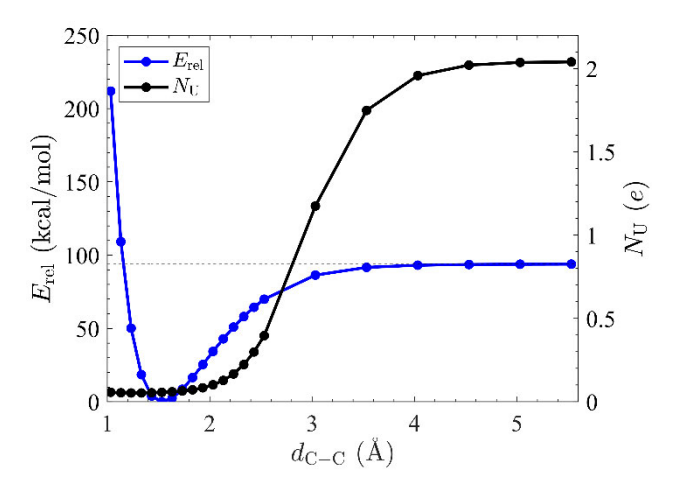


Figure 2. Potential energy curve (energies in relation to the minimum geometry) for relaxed displacement along the CC bond in ethane and N_U values calculated with MR-AQCC(PPMC).

The critical region of CC bond stretching occurs between 2 - 4 Å. Figure 3Figure 3 shows the evolution of the NO occupations with d_{C-C} in this region. At around 2 Å, the highest occupied NO (HONO) and lowest unoccupied NO (LUNO) have standard closed-shell occupations of two and zero, respectively. As the CC distance increases, HONO-LUNO occupations increasingly deviate from these values. Near the dissociation region, around 4 Å, the HONO and LUNO occupations are close to 1 e, indicating a strong correlation between the bonding and antibonding orbital pair.

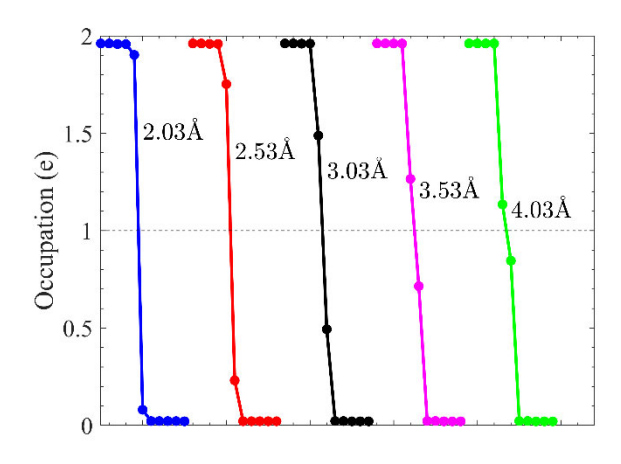


Figure 3. Natural orbitals occupation as a function of the CC bond distance for ethane calculated with MR-AQCC(PPMC).

The evolution of the corresponding total unpaired density with the CC displacement for ethane is displayed in Figure 4Figure 4. The unpaired density initially increases with d_{C-C} ; after a distance d_{C-C} of ~3 Å, the shape of the unpaired density no longer changes except to decrease the overlap between the two radical centers. The shape of the unpaired density initially resembles a hybrid sp^3 orbital at each carbon oriented along the CC bond. The dissociation process finally leads to the unpaired density of two CH₃ radicals.

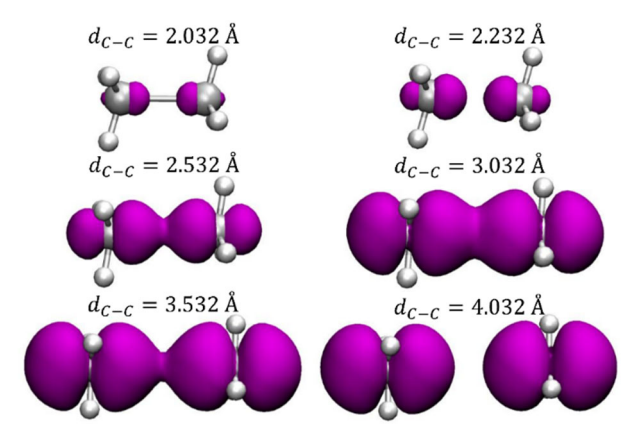


Figure 4. Unpaired density for ethane calculated with MR-AQCC (isovalue 0.003 $e \cdot \text{Å}^{-3}$).

The DFT potential energy curves for relaxed CC dissociation of ethane and the FT-DFT corresponding $N_{\rm FOD}$ values are shown in Figure 5Figure 5 for RDFT and UDFT calculations. Stability analysis was performed for all calculated geometries, and the RDFT method was found to be unstable for structures with $d_{\rm C-C} \ge 2.53$ Å. In these cases, UDFT and FT-UDFT calculations were also performed. The UDFT method, compared to RDFT, correctly describes the behavior of the dissociation energy, which converges to 96.5 kcal/mol, in good agreement with the MR-AQCC result. As expected, the RDFT method does not give the correct dissociation limit. The favorable dissociation properties of the UDFT method result from spin polarization, where the alpha and beta orbitals become localized in different parts of the molecule, as shown in Figure 6. In this figure, at a CC distance of 2.53 Å, both RDFT and UDFT methods show delocalized alpha and beta orbitals around both fragments. However, at 5.53 Å, the RDFT orbitals remain delocalized, while the UDFT method localizes the alpha orbitals in one fragment and the beta orbitals in the other. At the same time the RDFT HOMO-LUMO gap decreases significantly in

contrast to the UDFT case. This localization is crucial for accurately describing the dissociation process and the resulting radical species, as it allows the method to capture the static electron correlation and the correct electronic structure of the dissociated fragments. However, Figure 5 also shows that the N_{FOD} values computed with FT-UDFT remain around ~0.2 e for the entire dissociation process and do not reach the limit of 2 e expected for the biradical system. On the other hand, the N_{FOD} values are well described with the FT-RDFT method, reaching ~2 e in the dissociation region.

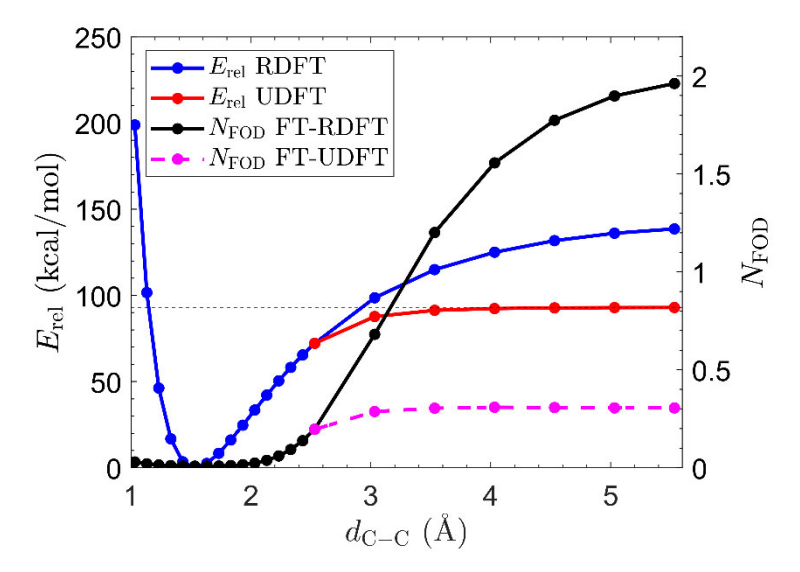


Figure 5. Potential energy curve for relaxed displacement (in relation to the minimum geometry) and FOD number ($T_{\rm el}$ of 9000 K) for the CC bond in the ethane molecule calculated with the B3LYP functional.

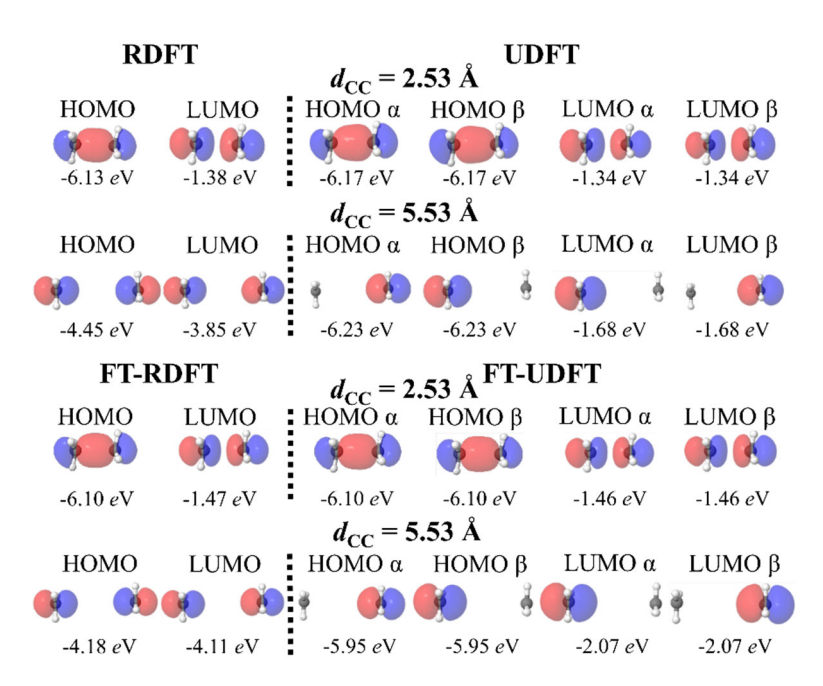


Figure 6. HOMO-LUMO orbitals of ethane molecule calculated with B3LYP functional (isovalue $0.1 e \cdot Å^{-3}$, $T_{el} = 9000 \text{ K}$ in FT-DFT methods).

The reason for this difference between RDFT and UDFT concerning N_{FOD} values lies in the different evolution of the HOMO-LUMO (H-L) gaps to cope with the static electron correlation. Figure S1 shows that this gap remains large both for UDFT and FT-UDFT and respective occupation numbers f_{LUMO} remain small (Table S1), leading to the unphysically small N_{FOD} values. RDFT cannot provide the correct dissociation limit but reduces the H-L gap toward zero (Figure S1) leading to the correct f_i occupations (Table S1). Unfortunately, both goals, correct energy dissociation and correct biradical character cannot be achieved in this case.

The diradical nature of the long CC bond in structure **2** is tested through bond elongation, as was performed for ethane. Figure 7 shows the potential energy curves for relaxed displacement relative to the initial geometry and the FOD numbers for the CC bond in this structure using the B3LYP functional. The structure at the minimum geometry has C_{2v} symmetry [31]. As has been shown previously [31], upon stretching the CC bond to around 2.3 Å within C_{2v} symmetry, the potential energy curve bifurcates, resulting in a new, more stable C_2 geometry with twisted fluorene groups. The N_{FOD} values for the C_2 structure show a rapid increase from \sim 1.6 e to 2.0 e, indicating the breaking of the CC bond due to reduced overlap between the carbon orbitals. With C_{2v} symmetry, the N_{FOD} increase is almost linear until reaching 2 e at 2.7 Å. The energy bifurcation and emergence of two distinct structures suggest the existence of a CC

bond until 2.2 Å, with a subsequent break occurring between 2.2-2.3 Å. Unlike what was found for ethane, $N_{\rm FOD}$ values obtained from both FT-RDFT and FT-UDFT methods remain practically the same for both $C_{\rm 2v}$ and $C_{\rm 2}$ structures, implying convergence of FT-UDFT to the FT-RDFT solution. This can be seen explicitly from the MO plots and orbital energies for $C_{\rm 2}$ (Figures S2 and S3) and for $C_{\rm 2v}$ (Figures S4 and S5) structures, which are identical for FT-RDFT and FT-UDFT for short and long distances.

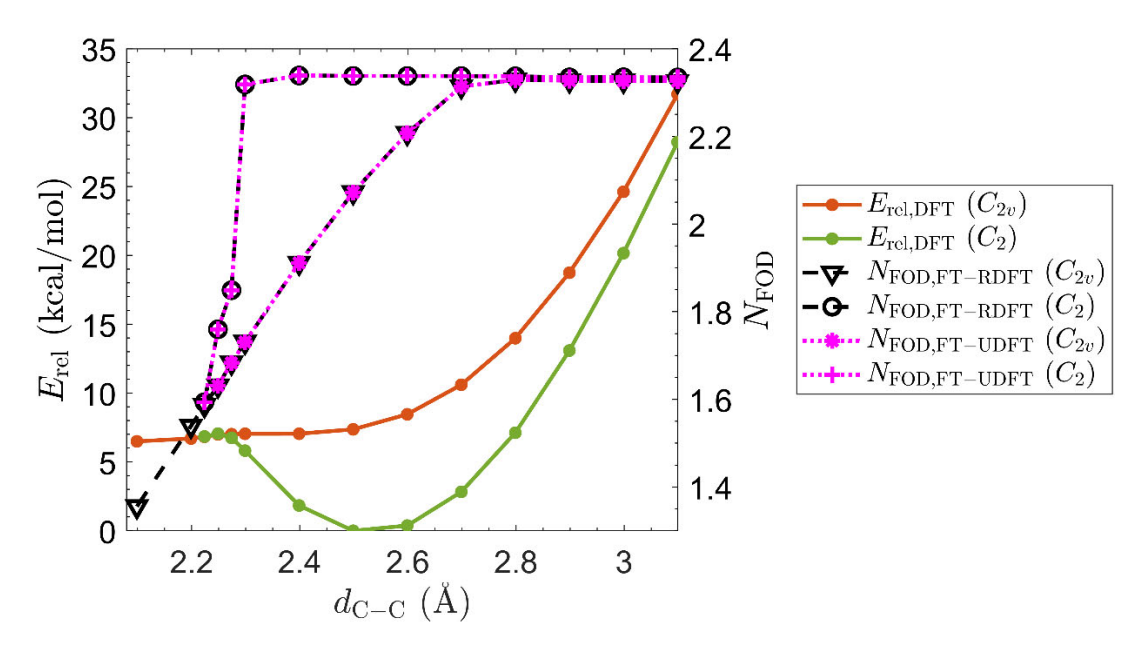


Figure 7. Potential energy curve for relaxed displacement (in relation to the minimum geometry) and FOD number ($T_{\rm el}$ of 9000K) for CC bond to structure 2 calculated at the UB3LYP level.

Figure S6 shows the MO diagram for structure **2** in C_2 symmetry. The UDFT H-L gap is smaller than in ethane (ethane at dissociation limit: 4.6 eV vs. structure 2: 1.9 eV). Therefore, the electronic temperature is high enough to occupy the LUMO, leading to the FT-RDFT solution. The same behavior is seen for structure **2** in C_{2v} symmetry (Figure S7). It is concluded that a small enough H-L gap in the original UDFT calculation can lead to a correct description of N_{FOD} values in FT-UDFT calculations.

3.2. CC double bond dissociation

Figure 8 illustrates the evolution of N_U values and the potential energy curve for the relaxed displacement of the CC double bond in ethylene using the MR-AQCC(GVB-RCI) approach. In the dissociation limit, the N_U value converges to 4.0 e, indicating that the radical

fragment CH₂ possesses two unpaired electrons, thus making the triplet state the ground state of this molecular radical fragment, in agreement with earlier results by Staemmler [60] and Brooks and Schaefer [61]. The corresponding dissociation energy D_e at the MR-AQCC(GVB-RCI) level is 171.8 kcal·mol⁻¹; D_θ is 161.65 kcal·mol⁻¹, in good agreement with the experimental value of 163.0 kcal·mol⁻¹ [62]. The D_e value using the GVB method given in Ref. [59] is 150.5 kcal/mol, again significantly underestimating the actual value. The analysis of the evolution of natural orbital (NO) occupations for ethylene is presented in Figure S8 in the SI. At the dissociation limit, the occupation of four NOs goes to 1 e, indicating the bond dissociation of both bonds. However, the occupation of the HONO and LUNO π orbitals approaches 1 e somewhat before the occupation of HONO-1 and LUNO+1 σ orbitals (Figure S9). This suggests that the π bond undergoes dissociation a bit before the σ bond. This phenomenon is attributed to the smaller lateral overlap of the atomic π orbitals, which is less efficient than the overlap of the CC sp² atomic orbitals.

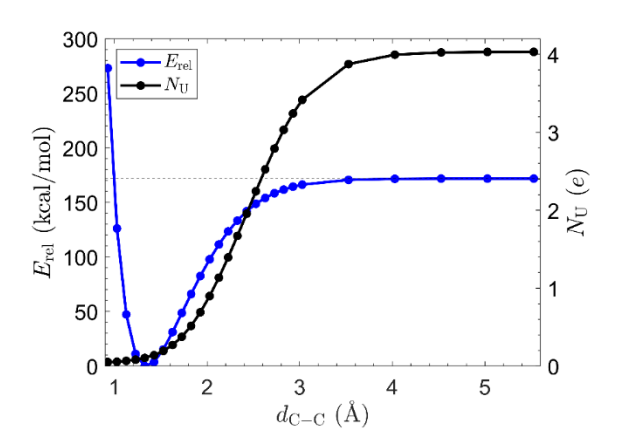


Figure 8. Potential energy curve for relaxed displacement (in relation to the minimum geometry) along the CC bond in ethylene and $N_{\rm U}$ values calculated with the MR-AQCC(GVB-RCI) method.

The DFT potential energy curves for relaxed CC dissociation of ethylene and the corresponding FT-DFT N_{FOD} values are shown in Figure 9. The UDFT method describes a smooth dissociation, while the RDFT shows a discontinuity around 3.5 Å. The FT-UDFT N_{FOD} values converge to 0.43 e FT-UDFT level, a value which is similar to the ethane result and is much too small. The asymptotic FT-RDFT N_{FOD} value is 2.30 e, a value which also falls short of the correct value of 4 e.

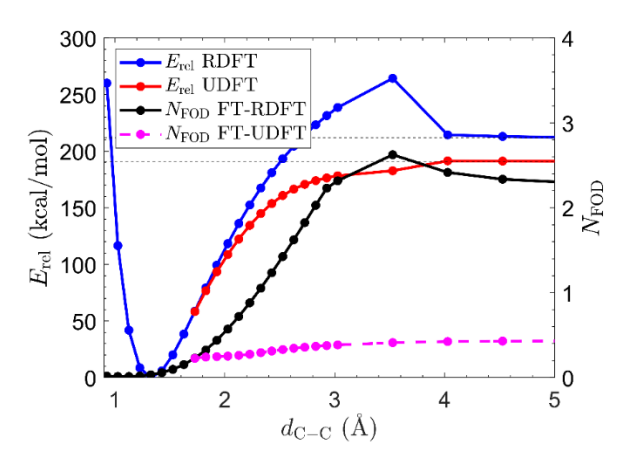


Figure 9. Potential energy curve for relaxed displacement (in relation to the minimum geometry) and FOD number ($T_{\rm el}$ of 9000 K) for the CC double bond in the ethylene molecule calculated with the B3LYP functional.

3.3. CC triple bond dissociation

The dissociation of acetylene along the CC triple bond produces two methylidyne radicals [61], each with a ${}^2\Pi$ doublet ground state with an orbital configuration $1\sigma^2 2\sigma^2 3\sigma^2 1\pi_x^1$ and an equivalent one for the π_y component. The GVB-RCI method restricts the construction of the total wavefunction using pairs of bonding and anti-bonding orbitals, forcing electrons to remain in the $(\sigma_g, \sigma_u)^2$, $(\pi_{xg}, \pi_{xu})^2$ and $(\pi_{yg}, \pi_{yu})^2$ electron pairs without the possibility of electron rearrangement, dissociating to the high-spin fragments. To allow for a correct dissociation, a valence MR-CISD(SA5-CAS(10,10)) was chosen and in total five electronic states were calculated to investigate avoided crossings (Figure S10). Figure 10 illustrates the MR-CISD ground state potential energy curve for acetylene and the evolution of N_U values. As expected, the $N_{\rm U}$ values increase up to approximately 5 e when the CC bond distance reaches 2.5 Å, correlating with dissociation into ${}^{4}\Sigma$ states. Around 2.5 Å, there is an avoided crossing among the 1¹A_g, 2¹A_g, and 3¹A_g states (Figure S10). Beyond this point, the N_U values fall to around 2 e due to the avoided crossing, which alters the ground state character to achieve the dissociation into $^{2}\Pi$ states of CH. The D_{e} value at MR-CISD level is 228.4 kcal/mol; with MR-CISD+P D_{e} is 218.8 kcal/mol and D_0 is 211.0 kcal/mol, the latter to be compared with the experimental value of 228.7 \pm 0.5 kcal/mol (via heat of formation) [63]. The GVB result of Ref. [59] ($D_e = 212.5$ kcal/mol) is again somewhat too low.

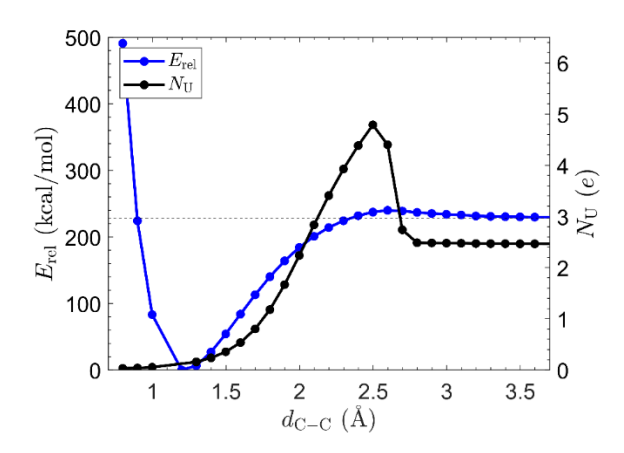


Figure 10. Potential energy curve for relaxed displacement (in relation to the minimum geometry) along the CC bond in acetylene and $N_{\rm U}$ values calculated with the MR-CISD(SA5-CAS(10,10)) method.

Figure 11 shows the DFT potential energy curve for relaxed CC dissociation of acetylene and the corresponding FT-DFT N_{FOD} values. Similar to ethane and ethylene, the UDFT method describes a smooth dissociation curve up to approximately 3 Å. At this distance, there is a small discontinuity, which comes from a sudden change in the orbital occupation. The dissociation limit is found at 232.5 kcal/mol without ZPE and 224.8 kcal/mol with ZPE correction, in good agreement with the experimental values of 228.7±0.5 kcal/mol [63]. In contrast, the RDFT method tends to dissociate to a much higher dissociation energy limit. However, at 3 Å, the RDFT energy curve also shows a sudden step-down showing convergence to the dissociation limit 280.1 kcal/mol, higher than the UDFT value. This unusual step behavior can be explained by analyzing the molecular orbitals of structures at 3.0 and 3.1 Å, where the abrupt change occurs. In the RDFT case, the σ_g and σ_u orbitals, initially HOMO-2 and LUMO at a CC bond distance of 3 Å (Figure S11), become HOMO-1 and HOMO-2 at a CC bond distance of 3.1 Å, resulting in four electrons in σ_g and σ_u and two in π_{yu} . A similar behavior is observed for UDFT (Figure S12). Regarding FT-DFT N_{FOD} values, both methods converge to 2 e. However, the FT-RDFT method shows a rearrangement between 2-2.5 Å, while FT-UDFT starts to converge to 2 e only around 2.5 Å.

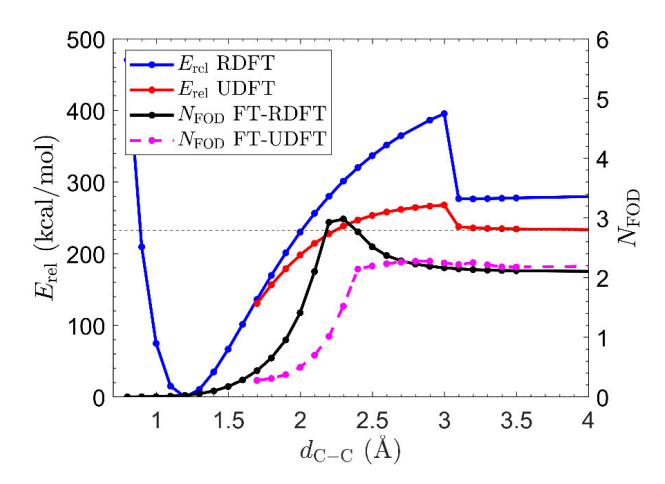


Figure 11. Potential energy curve for relaxed displacement (in relation to the minimum geometry) and FOD number (Tel of 9000 K) for the CC triple bond in the acetylene molecule calculated with the B3LYP functional.

3.4. Parameterization of $T_{\rm el}$ for range-separated and double hybrid functionals

Following the procedures adopted in the previous work [10], regression analysis was conducted for the following range-separated functionals ωB97XD, ωB97M-V, CAM-B3LYP, LC-ωPBE, and MN12-SX and the double hybrid functional B2PLYP to assess the overall agreement between the MR-AQCC N_U and FT-RDFT N_{FOD} values and to adjust T_{el} used for the FOD calculations. In the case of B2PLYP, only the DFT part has been considered for the FOD calculation but an extension to orbital-optimized double hybrids is already envisaged in our laboratories. Furthermore, the popular functional M06-2X has been added in addition to the previously considered M05-2X. The re-optimized regression formula for $T_{\rm el}$ in dependence of the Hartree-Fock exchange α_x developed in the previous work [10] is given as follows:

$$T_{el} = 10762 \, K \times a_r + 6140 \, K \tag{5}$$

 $T_{el} = 10762 \, K \times a_x + 6140 \, K$ (5) Table S2 presents the a_x values for all functionals analyzed here. Starting with the hybrid functional M06-2X, Figure S13 shows the regression plot between MR-AQCC Nu and FT-RDFT $N_{\rm FOD}$ values for structures 5-26 using the re-optimized $T_{\rm el}$ of 11900 K. In this figure, the regression data with the slope being 1.07 and R² being 0.98 are very good, which further supports the previously developed rule for defining $T_{\rm el}$ (Eq. (5)(5)) for hybrid functionals. Figure S14 demonstrates the good result of Eq. (5)(5) to T_{el} of the DFT portion of the double hybrid functional B2P-LYP, which has a slope of 1.03 and R² of 0.98.

Next, the important class of range-separated functionals is being investigated. The example of the $\omega B97XD$ functional shown in Figure 12a demonstrates that T_{el} value of 8530 K computed according to Eq. (5)(5) from the regression formula for exact Fock exchange is much too low. Further investigations on the other range-separated functionals (CAM-B3LYP, LC- ω PBE, MN12-SX, ω B97M-V) confirmed the finding (Figures S15a-S18a) that the previous temperature adjustment was not effective for this class of functionals. Therefore, a new $T_{\rm el}$ was derived for these functionals. Figure 12b shows the newly determined Fermi temperature for the ω B97XD functional. The R² value increased significantly from 0.89 to 0.98, while the slopes improved from 0.32 to 0.99. Similar good improvements were found for the remaining range-separated functionals (Figures S15b-S18b). The range separated functionals split the Coulomb operator into short-range (SR) and long-range (LR) parts, according to the equation [64, 65]:

$$\frac{1}{r_{12}} = \frac{1 - \left[\alpha + \beta \cdot \operatorname{erf}(\omega r_{12})\right]}{r_{12}} + \frac{\alpha + \beta \cdot \operatorname{erf}(\omega r_{12})}{r_{12}} \tag{6}$$

In this equation, the first term represents the SR part, while the second term represents the LR part. Here, ω is the range separation parameter, α represents the percentage of HF exchange in the short-range limit (a), and $\alpha+\beta$ is the corresponding percentage in the long-range limit. Linear correlation of the adjusted $T_{\rm el}$ for range-separated functionals was performed against the parameters α , $\alpha+\beta$ and β (Figures S19-S21). These figures show that an acceptable correlation of $T_{\rm el}$ exist only for the parameter β . $T_{\rm el}$ depends on the β parameter, with an R² value of 1.00, following the equation:

$$T_{el} = 6650 K \times \beta + 9010 K \tag{7}$$

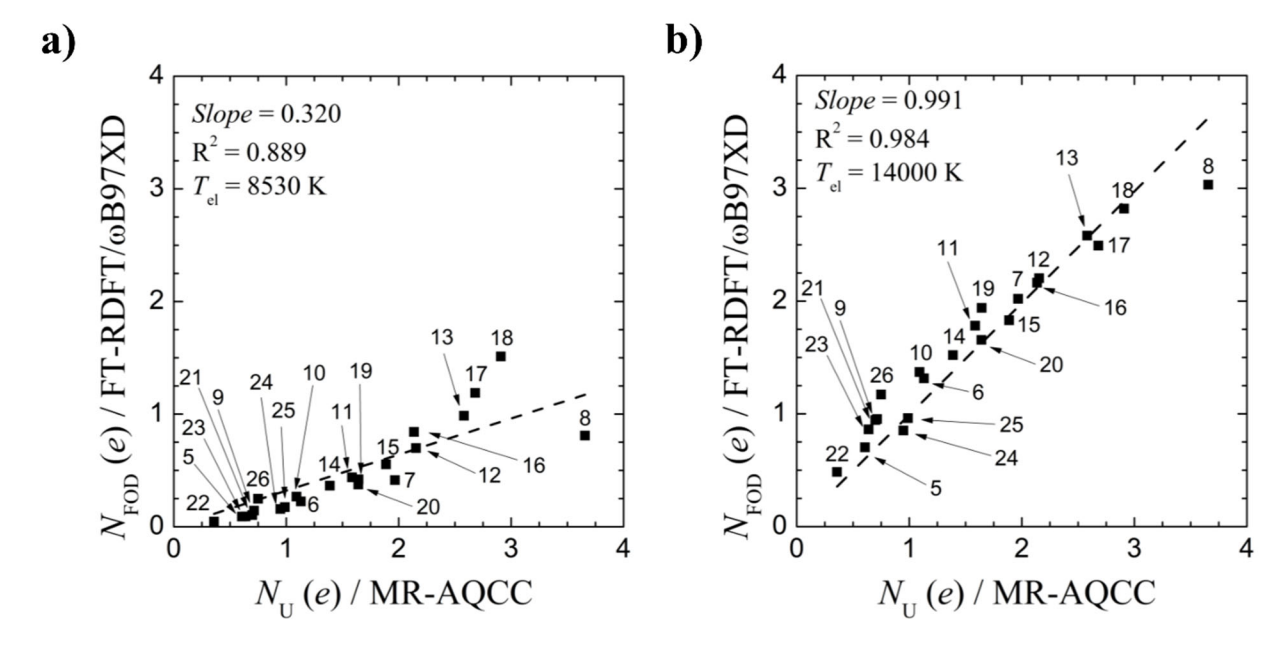


Figure 12. Comparison between MR-AQCC N_U values and FT-RDFT N_{FOD} numbers with ω B97XD density functional for structures with singlet ground electronic state (5-26, Figure 1) using the (a) T_{el} of Eq. (5)(5) of 8530 K and (b) improved-present T_{el} of 14000 K.

The semiempirical GFN2-xTB method, which has been investigated as last example, does not include non-local Fock exchange admixture a_x . Therefore, the previously adjusted equation for T_{el} in terms of a_x does not apply to GFN2-xTB. As a result, a new T_{el} was developed specifically for this methodology. The optimal temperature for this method was found to be 5200 K. Figure 13 shows the good correlation with MR-AQCC N_U values for structures 5-26.

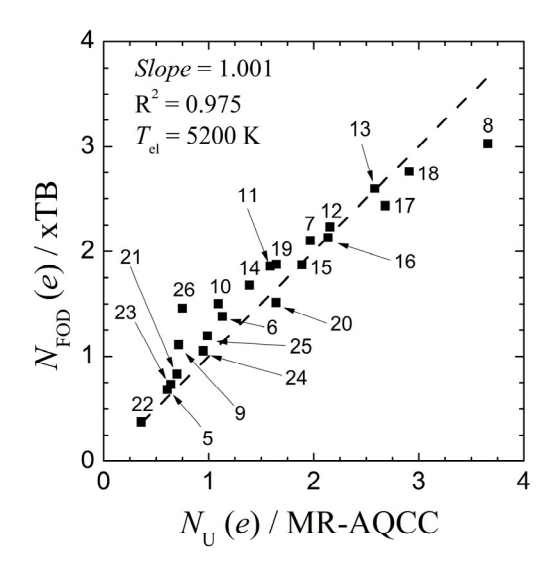


Figure 13. Comparison between MR-AQCC $N_{\rm U}$ values and FT-RDFT $N_{\rm FOD}$ numbers with GNF2-xTB method for structures with singlet ground electronic state (5-26, Figure 1) using the improved-present $T_{\rm el}$ of 5200 K.

4 CONCLUSION

In this work, we have considered two areas of multireference situations, one arising from bond dissociation and the other from PAH biradical character. We discuss as a major tool to characterize such processes the FOD analysis, which allows the occupation of low-lying virtual orbitals of a DFT calculation by means of an elevated electronic Fermi temperature $T_{\rm el}$. Inspired by the search for long covalent CC single bonds, we have chosen this case as one starting point and extended it by investigation of CC double and triple bonds, using ethylene and acetylene, respectively, as examples. The remarkable biradical properties of PAHs formed the second application field.

Assessment of the validity of DFT calculations in these fields is not recommended without independent verification. For that purpose, the MR-AQCC and MR-CISD methods have been selected, which take the open-shell character into account by design. The unpaired densities are the direct counterpart of the FODs. Many factors work very well at the DFT level. However, there is an interesting caveat. For the energetics of dissociation processes, usually UDFT has to be employed. UDFT manages the static electron correlation problem (quasi degeneracies mentioned above) by symmetry breaking of molecular orbitals. As a consequence, HOMO-LUMO gaps can remain large, which does not allow sufficient occupation of the LUMO at the

FT-DFT level. Consequently, the FOD values remain unphysically low. This behavior has been observed for ethane and ethylene. On the other hand, RDFT (which gives a wrong dissociation behavior) reacts on the dissociation by decreasing the HOMO-LUMO gap of delocalized orbitals, leading to essentially correct FOD values. Thus, as these examples show, it will not always be possible to obtain the correct simultaneous description of FOD open shell character and potential energy dissociation curves. However, it seems that most of the cases investigated here are not critical so that UDFT calculations are often achieving both mentioned goals at the same time.

The second task of this work was dedicated to a practical, but nevertheless important problem: the determination of the adequate Fermi temperature $T_{\rm el}$ for different functionals. The hybrid (M06-2X) and double hybrid (B2P-LYP) functionals tested in this work showed good correlation between N_{FOD} and N_{U} values when using the improved T_{el} from previous studies [10]. For range-separated functionals, a new adjustment had to be made, correlating $T_{\rm el}$ with the parameter β , which represents the difference between the percentage of HF exchange in the longrange limit and the short-range limit. A new linear regression between $T_{\rm el}$ and β is proposed. For the semi-empirical GFN2-xTB method, our findings suggest an optimal temperature of 5200 K. At this point, it should also be pointed out again that the partial summation over occupied and virtual orbitals (referred to as pseudo-occupied and pseudo-virtual in Ref. [66]) is performed separately in the FOD method. However, the two values agree numerically very well within two decimal places (see SI, Table S3 for examples), which is consistent with the conclusions of Ref. [66], i.e., in principle one could also consider only the occupied orbitals in the summation and then multiply the values by two. This perfectly reflects the symmetric nature of particles and holes and is also confirmed by effective numbers of unpaired electrons based on MR-AQCC, albeit slightly less precisely (see SI, Table S3).

In summary, we have shown that the FOD analysis provides a versatile and useful tool to quickly assess the open shell character of organic compounds by means of FT-DFT calculations using several types of functionals. The comparison with reference MR-AQCC results allowed us to determine the electronic temperature in an unambiguous way. The FOD calculations can be performed routinely based on available FT-DFT calculations. In our investigations we found only a few cases of complete bond dissociation where the FT-UDFT version did not work, but RDFT gave the correct results.

Supporting Information

The online version contains supporting information on the PECs, molecular orbitals, $N_{\rm U}$ and FOD values for ethane, 9,9'-(ethene-1,1-diyl)bis(9H-fluorene), ethylene and acetylene, and comparison between $N_{\rm U}$ and FOD values for the PAH structures and density functionals investigated in this work.

Conflict of Interest

There are no conflicts to declare.

Data Availability

Data is provided within the manuscript or Supporting Information files.

ACKNOWLEDGEMENTS

Support by the U.S. National Science Foundation for this research (H. L.: Grant No. CHE-2107923, M. K.: Grant No. CHE-2107820) is gratefully acknowledged. We are grateful for the supply of ample computer time at the HPCC facilities of Texas Tech University.

REFERENCES

- [1] T. Kubo, Y. Suga, D. Hashizume, H. Suzuki, T. Miyamoto, H. Okamoto, R. Kishi, M. Nakano (2021) Long Carbon–Carbon Bonding beyond 2 Å in Tris(9-fluorenylidene)methane. J Am Chem Soc 143: 14360-14366.
- [2] Y. Ishigaki, T. Shimajiri, T. Takeda, R. Katoono, T. Suzuki (2018) Longest C–C single bond among neutral hydrocarbons with a bond length beyond 1.8 Å. Chem 4: 795-806.
- [3] H. Kawai, T. Takeda, K. Fujiwara, T. Inabe, T. Suzuki (2005) Exceptionally Large Difference in Bond Length among Conformational Isomorphs of a Hexaphenylethane Derivative with a Dispiropyracene Skeleton. Cryst Growth Des 5: 2256-2260.
- [4] F. Toda, K. Tanaka, Z. Stein, I. Goldberg (1996) Extremely Long C-C Bonds in Strained 1,1,2,2-Tetraphenylcyclobutaarenes: 3,8-Dichloro-1,1,2,2-tetraphenylcyclobuta[b]naphthalene, C36H24Cl2, and 3,6,9,10-Tetrachloro-4,5-dimethyl-1,1,2,2,7,7,8,8-octaphenyldicyclobuta[b,h]phenanthrene Toluene Solvate, C68H46Cl4.1.5C7H8. Acta Cryst C 52: 177-180.
- [5] S. Kammermeier, R. Herges, P.G. Jones (1997) [2+2] Cycloaddition Products of Tetradehydrodianthracene: Experimental and Theoretical Proof of Extraordinary Long C-C Single Bonds. Angew Chem Int Ed 36: 1757-1760.
- [6] K. Tanaka, N. Takamoto, Y. Tezuka, M. Kato, F. Toda (2001) Preparation and structural study of naphtho- and anthrocyclobutene derivatives which have extremely long C–C bonds. Tetrahedron 57: 3761-3767.
- [7] P.R. Schreiner, L.V. Chernish, P.A. Gunchenko, E.Y. Tikhonchuk, H. Hausmann, M. Serafin, S. Schlecht, J.E.P. Dahl, R.M.K. Carlson, A.A. Fokin (2011) Overcoming lability of extremely long alkane carbon–carbon bonds through dispersion forces. Nature 477: 308-311.
- [8] S. Grimme, P.R. Schreiner (2011) Steric Crowding Can Stabilize a Labile Molecule: Solving the Hexaphenylethane Riddle. Angew Chem Int Ed 50: 12639-12642.
- [9] P.G. Szalay, T. Müller, G. Gidofalvi, H. Lischka, R. Shepard (2012) Multiconfiguration Self-Consistent Field and Multireference Configuration Interaction Methods and Applications. Chem Rev 112: 108-181.
- [10] R. Nieman, J.R. Carvalho, B. Jayee, A. Hansen, A.J.A. Aquino, M. Kertesz, H. Lischka (2023) Polyradical character assessment using multireference calculations and comparison with density-functional derived fractional occupation number weighted density analysis. Phys Chem Chem Phys 25: 27380-27393.
- [11] C.A. Bauer, A. Hansen, S. Grimme (2017) The Fractional Occupation Number Weighted Density as a Versatile Analysis Tool for Molecules with a Complicated Electronic Structure. Chem Eur J 23: 6150-6164.
- [12] B.-J. Chen, J.-D. Chai (2022) TAO-DFT fictitious temperature made simple. RSC Advances 12: 12193-12210.
- [13] F. Liu, C. Duan, H.J. Kulik (2020) Rapid Detection of Strong Correlation with Machine Learning for Transition-Metal Complex High-Throughput Screening. J Phys Chem Lett 11: 8067-8076.
- [14] J.-D. Chai (2012) Density functional theory with fractional orbital occupations. J Chem Phys 136: 154104.
- [15] J.-D. Chai (2014) Thermally-assisted-occupation density functional theory with generalized-gradient approximations. J Chem Phys 140: 18A521.

- [16] J.-D. Chai (2017) Role of exact exchange in thermally-assisted-occupation density functional theory: A proposal of new hybrid schemes. J Chem Phys 146: 044102.
- [17] K. Takatsuka, T. Fueno, K. Yamaguchi (1978) Distribution of odd electrons in ground-state molecules. Theor Chim Acta 48: 175-183.
- [18] V.N. Staroverov, E.R. Davidson (2000) Distribution of effectively unpaired electrons. Chem Phys Lett 330: 161-168.
- [19] M. Head-Gordon (2003) Characterizing unpaired electrons from the one-particle density matrix. Chem Phys Lett 372: 508-511.
- [20] E. Ramos-Cordoba, P. Salvador, E. Matito (2016) Separation of dynamic and nondynamic correlation. Phys Chem Chem Phys 18: 24015-24023.
- [21] E. Ramos-Cordoba, E. Matito (2017) Local Descriptors of Dynamic and Nondynamic Correlation. J Chem Theory Comput 13: 2705-2711.
- [22] R.J. Bartlett, Y.C. Park, N.P. Bauman, A. Melnichuk, D. Ranasinghe, M. Ravi, A. Perera (2020) Index of multi-determinantal and multi-reference character in coupled-cluster theory. J Chem Phys 153.
- [23] S. Grimme, A. Hansen (2015) A practicable real-space measure and visualization of static electron-correlation effects. Angew Chem Int Ed 54: 12308-12313.
- [24] P.G. Szalay, R.J. Bartlett (1993) Multi-reference averaged quadratic coupled-cluster method: a size-extensive modification of multi-reference CI. Chem Phys Lett 214: 481-488.
- [25] J. Tao, J.P. Perdew, V.N. Staroverov, G.E. Scuseria (2003) Climbing the Density Functional Ladder: Nonempirical Meta--Generalized Gradient Approximation Designed for Molecules and Solids. Phys Rev Lett 91: 146401.
- [26] C. Lee, W. Yang, R.G. Parr (1988) Development of the Colle-Salvetti correlation-energy formula into a functional of the electron density. Phys Rev B 37: 785-789.
- [27] A.D. Becke (1993) Density-functional thermochemistry. III. The role of exact exchange. J Chem Phys 98: 5648-5652.
- [28] Y. Zhao, N.E. Schultz, D.G. Truhlar (2006) Design of Density Functionals by Combining the Method of Constraint Satisfaction with Parametrization for Thermochemistry, Thermochemical Kinetics, and Noncovalent Interactions. J Chem Theory Comput 2: 364-382.
- [29] C. Bannwarth, E. Caldeweyher, S. Ehlert, A. Hansen, P. Pracht, J. Seibert, S. Spicher, S. Grimme (2021) Extended tight-binding quantum chemistry methods. WIREs Comp Mol Sci 11: e1493.
- [30] C. Bannwarth, S. Ehlert, S. Grimme (2019) GFN2-xTB—An Accurate and Broadly Parametrized Self-Consistent Tight-Binding Quantum Chemical Method with Multipole Electrostatics and Density-Dependent Dispersion Contributions. J Chem Theory Comput 15: 1652-1671.
- [31] E.J.J. Korpela, J.R. Carvalho, H. Lischka, M. Kertesz (2023) Extremely Long C–C Bonds Predicted beyond 2.0 Å. J Phys Chem A 127: 4440-4454.
- [32] J.-D. Chai, M. Head-Gordon (2008) Long-range corrected hybrid density functionals with damped atom—atom dispersion corrections. Phys Chem Phys 10: 6615-6620.
- [33] J.-D. Chai, M. Head-Gordon (2008) Systematic optimization of long-range corrected hybrid density functionals. J Chem Phys 128: 084106.
- [34] N. Mardirossian, M. Head-Gordon (2016) ωB97M-V: A combinatorially optimized, range-separated hybrid, meta-GGA density functional with VV10 nonlocal correlation. J Chem Phys 144: 214110.

- [35] T. Yanai, D.P. Tew, N.C. Handy (2004) A new hybrid exchange–correlation functional using the Coulomb-attenuating method (CAM-B3LYP). Chem Phys Lett 393: 51-57.
- [36] O.A. Vydrov, G.E. Scuseria (2006) Assessment of a long-range corrected hybrid functional. J Chem Phys 125: 234109.
- [37] R. Peverati, D.G. Truhlar (2012) Screened-exchange density functionals with broad accuracy for chemistry and solid-state physics. Phys Chem Chem Phys 14: 16187-16191.
- [38] S. Grimme (2006) Semiempirical hybrid density functional with perturbative second-order correlation. J Chem Phys 124: 034108.
- [39] Y. Zhao, D.G. Truhlar (2008) The M06 suite of density functionals for main group thermochemistry, thermochemical kinetics, noncovalent interactions, excited states, and transition elements: two new functionals and systematic testing of four M06-class functionals and 12 other functionals. Theor Chem Acc 120: 215-241.
- [40] R. Shepard (1987) The multiconfiguration self-consistent field method. Ab Initio Methods in Quantum Chemistry–II 63.
- [41] L.B. Harding, W.A. Goddard III (1975) Generalized valence bond description of the low-lying states of formaldehyde. J Am Chem Soc 97: 6293-6299.
- [42] T.H. Dunning Jr, D.C. Cartwright, W.J. Hunt, P.J. Hay, F.W. Bobrowicz (1976) Generalized valence bond calculations on the ground state (X 1Σ + g) of nitrogen. J Chem Phys 64: 4755-4766.
- [43] R. Shepard, G.S. Kedziora, H. Lischka, I. Shavitt, T. Müller, P.G. Szalay, M. Kállay, M. Seth (2008) The accuracy of molecular bond lengths computed by multireference electronic structure methods. Chemical Physics 349: 37-57.
- [44] R. Krishnan, J.S. Binkley, R. Seeger, J.A. Pople (1980) Self-consistent molecular orbital methods. XX. A basis set for correlated wave functions. J Chem Phys 72: 650-654.
- [45] A.D. McLean, G.S. Chandler (1980) Contracted Gaussian basis sets for molecular calculations. I. Second row atoms, Z=11-18. J Chem Phys 72: 5639-5648.
- [46] F. Weigend, R. Ahlrichs (2005) Balanced basis sets of split valence, triple zeta valence and quadruple zeta valence quality for H to Rn: Design and assessment of accuracy. Phys Chem Chem Phys 7: 3297-3305.
- [47] F. Weigend (2006) Accurate Coulomb-fitting basis sets for H to Rn. Phys Chem Chem Phys 8: 1057-1065.
- [48] J. Čížek, J. Paldus (1967) Stability Conditions for the Solutions of the Hartree—Fock Equations for Atomic and Molecular Systems. Application to the Pi-Electron Model of Cyclic Polyenes. J Chem Phys 47: 3976-3985.
- [49] R. Bauernschmitt, R. Ahlrichs (1996) Stability analysis for solutions of the closed shell Kohn–Sham equation. J Chem Phys 104: 9047-9052.
- [50] R. Ahlrichs, M. Bär, M. Häser, H. Horn, C. Kölmel (1989) Electronic structure calculations on workstation computers: The program system turbomole. Chem Phys Lett 162: 165-169.
- [51] S.G. Balasubramani, G.P. Chen, S. Coriani, M. Diedenhofen, M.S. Frank, Y.J. Franzke, F. Furche, R. Grotjahn, M.E. Harding, C. Hättig, A. Hellweg, B. Helmich-Paris, C. Holzer, U. Huniar, M. Kaupp, A. Marefat Khah, S. Karbalaei Khani, T. Müller, F. Mack, B.D. Nguyen, S.M. Parker, E. Perlt, D. Rappoport, K. Reiter, S. Roy, M. Rückert, G. Schmitz, M. Sierka, E. Tapavicza, D.P. Tew, C. van Wüllen, V.K. Voora, F. Weigend, A. Wodyński, J.M. Yu (2020) TURBOMOLE: Modular program suite for ab initio quantum-chemical and condensed-matter simulations. J Chem Phys 152: 184107.

- [52] F. Neese, F. Wennmohs, U. Becker, C. Riplinger (2020) The ORCA quantum chemistry program package. J Chem Phys 152: 224108.
- [53] F. Neese (2022) Software update: The ORCA program system—Version 5.0. WIREs Comp Mol Sci 12: e1606.
- [54] H. Lischka, R. Shepard, T. Müller, P.G. Szalay, R.M. Pitzer, A.J.A. Aquino, M.M. Araújo do Nascimento, M. Barbatti, L.T. Belcher, J.-P. Blaudeau, I. Borges, S.R. Brozell, E.A. Carter, A. Das, G. Gidofalvi, L. González, W.L. Hase, G. Kedziora, M. Kertesz, F. Kossoski, F.B.C. Machado, S. Matsika, S.A. do Monte, D. Nachtigallová, R. Nieman, M. Oppel, C.A. Parish, F. Plasser, R.F.K. Spada, E.A. Stahlberg, E. Ventura, D.R. Yarkony, Z. Zhang (2020) The generality of the GUGA MRCI approach in COLUMBUS for treating complex quantum chemistry. J Chem Phys 152: 134110.
- [55] H. Lischka, T. Müller, P.G. Szalay, I. Shavitt, R.M. Pitzer, R. Shepard (2011) Columbus—a program system for advanced multireference theory calculations. Wires Comput Mol Sci 1: 191-199.
- [56] H. Dachsel, H. Lischka, R. Shepard, J. Nieplocha, R.J. Harrison (1997) A massively parallel multireference configuration interaction program: The parallel COLUMBUS program. J Comput Chem 18: 430-448.
- [57] K. Kuchitsu (1968) Comparison of Molecular Structures Determined by Electron Diffraction and Spectroscopy. Ethane and Diborane. J Chem Phys 49: 4456-4462.
- [58] F. Stahl, P.v.R. Schleyer, H. Jiao, H.F. Schaefer, K.-H. Chen, N.L. Allinger (2002) Resurrection of Neutral Tris-homoaromaticity. J Org Chem 67: 6599-6611.
- [59] T.H. Dunning, Jr., L.T. Xu, T.Y. Takeshita, B.A. Lindquist (2016) Insights into the Electronic Structure of Molecules from Generalized Valence Bond Theory. J Phys Chem A 120: 1763-1778.
- [60] V. Staemmler (1973) Ab initio calculations on small hydrides including electron correlation. Theor Chim Acta 31: 49-61.
- [61] B.R. Brooks, H.F. Schaefer, III (1977) Reactions of carbynes. Potential energy surfaces for the doublet and quartet methylidyne (CH) reactions with molecular hydrogen. J Chem Phys 67: 5146-5151.
- [62] S.W. Benson (1965) III Bond energies. J Chem Educ 42: 502.
- [63] K.M. Ervin, S. Gronert, S. Barlow, M.K. Gilles, A.G. Harrison, V.M. Bierbaum, C.H. DePuy, W. Lineberger, G.B. Ellison (1990) Bond strengths of ethylene and acetylene. J Am Chem Soc 112: 5750-5759.
- [64] T. Tsuneda, K. Hirao (2014) Long-range correction for density functional theory. WIREs Comp Mol Sci 4: 375-390.
- [65] G. Santra, R. Calinsky, J.M.L. Martin (2022) Benefits of Range-Separated Hybrid and Double-Hybrid Functionals for a Large and Diverse Data Set of Reaction Energies and Barrier Heights. J Phys Chem A 126: 5492-5505.
- [66] X. Xu, L. Soriano-Agueda, X. López, E. Ramos-Cordoba, E. Matito (2024) All-Purpose Measure of Electron Correlation for Multireference Diagnostics. J Chem Theory Comput 20: 721-727.